

valves presently appear to be a synapomorphy of post-Paleozoic discinids because tablet imprints have been found on fossil discinids but not on supposedly ancestral, Paleozoic orbiculoids (2). The larval shell of fossil discinoids, however, merits reinvestigation because imprints, which are seldom more than 50 nm deep, are commonly affected by degradation in living species and could be further obscured during fossilization. Moreover, larval shells of other early Paleozoic brachiopods with organophosphatic shells, the acrotretides (13–15) and the lingulides *Paterula* (15) and botsfordioids (16), bear imprints, ranging in size from 0.2 to over 2  $\mu\text{m}$  in close-packed hexagonal arrays. These imprints have been interpreted as impressions of thickly coated vesicles (13) forming an organic cover analogous to the vesicular periostracum of terebratellids (17). There are, however, two kinds of imprints. Some, like those on botsfordioid larval shells (16), are hemispherical and could have been moulds of vesicles accumulating beneath an external pellicle. Many acrotretide imprints, however, are shallow and flat-bottomed (Fig. 4B) (4, 18, 19) and could also have been made, like those ornamenting living discinid larvae, by biomineralized, possibly siliceous, tablets. There is presently no evidence of direct descent of living discinids from this ancient

stock, and it is possible, although unlikely, that the association between silica and apatite evolved more than once in brachiopod phylogeny.

The only siliceous metazoan remains recorded from the Early Cambrian (or indeed throughout the geological record) are the intracellularly secreted spicules of sponges, suggesting that metazoan ability to secrete silica was restricted (20). However, degradable siliceous mosaics like those forming the larval shell of apatitic discinids might have been developed in other phyla but recorded on their fossils simply as superficial imprints and hitherto overlooked as indicators of biomineralization.

#### REFERENCES AND NOTES

1. A. Williams *et al.*, in *Introduction*, vol. 1 of *Treatise on Invertebrate Paleontology: Part H, Brachiopoda*, R. Kaesler, Ed. (Geological Society of America and Univ. of Kansas Press, New York, and Lawrence, KS, 1997).
2. A. Williams, M. Cusack, J. O. Buckman, *Philos. Trans. R. Soc. London Ser. B.*, in press.
3. Glycosaminoglycans (GAGs), formerly known as mucopolysaccharides, are the principal component of the outer primary layer of the post-larval organophosphatic brachiopod shell.
4. L. E. Holmer, *Fossils Strata* **26**, 1 (1989).
5. The larval surfaces of atmospherically dried immature dorsal valves of *D. tenuis* were irrigated with acetone. Strips of cellulose acetate film (10  $\mu\text{m}$  thick) were placed on top and then peeled off, removing some biomineralized tablets.
6. The strips were carbon-coated and examined in a Cambridge 360 SEM (operating voltage = 20 kV, probe current = 132 pA).
7. Wavelength-dispersive maps for silicon and calcium were obtained by a JEOL superprobe (JXA 8900RL) on a gold-coated surface of the larval shell of *D. tenuis* (accelerating voltage = 8 kV, beam current = 6 nA, dwell time per pixel = 30 ms).
8. Dorsal valves of *D. tenuis* were incubated with the serine proteinase, subtilisin (E.C. 3.4.21.4) (2  $\mu\text{M}$ ) in sodium phosphate buffer (50 mM, pH 7.2), chitinase (E.C. 3.2.1.14) (1  $\mu\text{M}$ ) in sodium phosphate buffer (50 mM, pH 7.2), or an aqueous solution of sodium hypochlorite (bleach) (0.2% v/v) for 24 hours at 22°C. Solutions were removed and the specimens dried in a laminar-flow cabinet before gold coating for SEM study.
9. S. Mann and C. C. Perry, in *Silicon Biochemistry*, D. Evered and M. O'Connor, Eds. (Wiley, Chichester, UK, 1986), pp. 40–58.
10. W. J. Landis, D. D. Lee, J. T. Brenna, S. Chandra, G. H. Morrison, *Calcif. Tissue Int.* **38**, 52 (1986).
11. P. Li, C. Ohtsuki, T. Kokubo, K. Nakanishi, N. Soga, *J. Am. Ceram. Soc.* **75**, 2094 (1992).
12. K. Ohiura *et al.*, *J. Biomed. Mater. Res.* **25**, 357 (1991).
13. G. Biernat and A. Williams, *Palaeontology* **13**, 98 (1970).
14. A. Williams and L. E. Holmer, *ibid.* **35**, 657 (1992).
15. L. Popov, J. Nölvak, L. E. Holmer, *ibid.* **37**, 627 (1994).
16. L. E. Holmer, L. E. Popov, R. Wrona, *Palaeontol. Pol.* **55**, 37 (1996).
17. A. Williams and S. MacKay, *Proc. R. Soc. London Ser. B* **202**, 191 (1978).
18. R. Ludvigsen, *Neues Jahrb. Geol. Palaeontol. Monh.* **3**, 133 (1974).
19. A. Williams and G. B. Curry, in *Brachiopods Through Time*, D. I. MacKinnon, D. E. Lee, J. D. Campbell, Eds. (Balkema, Rotterdam, 1991), pp. 133–140.
20. H. A. Lowenstam and S. Weiner, *On Biomineralization* (Oxford Univ. Press, New York, 1989), p. 324.
21. Financial support from The Royal Society of London and the Natural Environment Research Council is greatly appreciated.

2 December 1997; accepted 12 February 1998

## Anomalous Strain Accumulation in the Yucca Mountain Area, Nevada

Brian Wernicke, James L. Davis, Richard A. Bennett, Pedro Elósegui, Mark J. Abolins, Robert J. Brady, Martha A. House, Nathan A. Niemi, J. Kent Snow

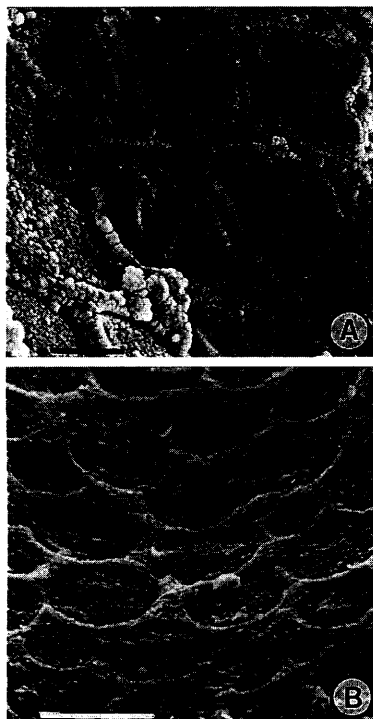


**Fig. 4.** Comparison of the imprints on larval shell surfaces made by (A) tablets of proteinaceous silica in living *Pelagodiscus atlanticus* (King) and (B) tablets of unknown composition in Late Cambrian *Linnarssonella girtyi* Walcott, Wilberns Formation, Texas. Bar, 0.5  $\mu\text{m}$  (A) and 5  $\mu\text{m}$  (B).

Global Positioning System (GPS) surveys from 1991 to 1997 near Yucca Mountain, Nevada, indicate west-northwest crustal elongation at a rate of  $1.7 \pm 0.3$  millimeters per year ( $1\sigma$ ) over 34 kilometers, or  $50 \pm 9$  nanostrain per year. Global Positioning System and trilateration surveys from 1983 to 1997 on a 14-kilometer baseline across the proposed repository site for high-level radioactive waste indicate that the crust extended by 0.7 to  $0.9 \pm 0.2$  millimeter per year ( $50$  to  $64 \pm 14$  nanostrain per year), depending on the coseismic effect of the  $M_s$  5.4 1992 Little Skull Mountain earthquake. These strain rates are at least an order of magnitude higher than would be predicted from the Quaternary volcanic and tectonic history of the area.

Strain buildup on major plate boundary fault zones appears to be relatively continuous between major earthquakes, which recur every few centuries. But is this also true of faults in more diffusely deforming intraplate settings, where recurrence intervals are several to tens of millennia? Or does strain accumulate rapidly in brief episodes,

perhaps migrating from region to region? The answer is fundamental to the physics of the earthquake cycle and for hazards assessment, but has remained elusive because of the difficulty of measuring the low strain rates characteristic of intraplate settings. Here we use GPS measurements to examine this issue near Yucca Mountain, Nevada.

Yucca Mountain is under consideration as a site for permanent disposal of high-level radioactive waste. An important consideration in evaluating the site is whether tectonic or volcanic events might cause the release of unacceptable amounts of radioactivity into the environment over the lifetime of the repository (the next 10,000 to 100,000 years). If the area is within an interval of accelerated activity, then the potential hazards would be underestimated on the basis of the long-term geologic record.

Yucca Mountain is one of numerous range blocks situated in the Basin and Range province, a wide region of diffuse intraplate strain characterized by roughly east-west to northwest-southeast tectonic extension and shear. Both Yucca Mountain and Little Skull Mountain to the east (Fig. 1) contain a set of north-trending, domino-like fault blocks. Most of the exposed rocks are middle Miocene [ $\sim 13$  million years ago (Ma)] pyroclastic flows that have been tilted gently eastward along west- to northwest-dipping normal faults (1, 2).

The basis for volcanic hazards assessment are several Quaternary, low-volume basaltic eruption centers near the proposed repository site (3). Four centers on Crater Flat, crudely aligned parallel to the faults at Yucca Mountain, developed at  $\sim 1.0$  Ma (4), and a fifth at the southern terminus of Yucca Mountain (Lathrop Wells cone) developed between 0.01 and 0.14 Ma [Fig. 1 (4, 5)]. The principal seismic hazards are: (i) the active Bare Mountain fault [Fig. 1 (6, 7)], (ii) Quaternary faults within or near the repository site (8), and (iii) active faults in the Jackass Flats area, based on the 29 June 1992  $M_s$  5.4 Little Skull Mountain earthquake (9, 10).

Determining the contemporary deformation rates in the area is a direct approach to addressing these hazards. A trilateration network centered on Yucca Mountain, occupied in 1983, 1984, and 1993 by the U.S. Geological Survey (USGS) indicated that east-west extension across the region was  $<50$  nanostrain per year (nstr/year) ( $<2.5$  mm/yr across an aperture of 50 km); the uncertainties in the data allowed that there was no motion (11).

To improve on these estimates, we conducted GPS surveys beginning in 1991 of an array of five geodetic markers crossing the proposed repository site, from Bare Mountain to Jackass Flats (12) (Fig. 1).

Stress measurements in boreholes on Yucca Mountain indicate that the stress regime is one of nearly pure normal faulting and that the least principal stress is oriented  $N60^\circ-65^\circ W$  (13). The GPS array was oriented parallel to this direction and to the mean tensional axis of the Little Skull Mountain earthquake sequence (9), and perpendicular to the north to northwest strike of mapped normal faults and the trend of the 1.0 Ma volcanic centers on Crater Flat (Fig. 1). The expected secular strain field from these tectonic and magmatic features is west-northwest extension.

The GPS surveys from 1991 to 1997 (Figs. 2 and 3) show that all four southeastern sites moved significantly ( $>99\%$  confidence) eastward to southeastward at  $1.0 \pm 0.3$  to  $1.7 \pm 0.3$  mm/year (scaled 1 $\sigma$

errors) relative to Claim (Fig. 3A) (14). Moreover, velocities appear to have increased southeastward in rough proportion to the distance from Claim (Fig. 3B); this pattern suggests that extension of  $\sim 50$  nstr/year has been uniform across the 34 km aperture of the network. The GPS results are thus in agreement with the expected strain field, and confirm an upper bound of east-west motion of  $\sim 2.5$  mm/year from the USGS results (11).

Two sites in our array, Wahomie and Mile, are also part of the USGS network. They define a  $\sim 14$  km baseline that crosses the proposed repository site (Fig. 1). We surveyed this baseline seven times between 1991 and 1997, and combined the results with the USGS surveys, yielding a time series of baseline lengths that includes a total

**Fig. 1.** Map showing distribution of pre-Quaternary bedrock (dot pattern), geodetic sites (triangles), and low-volume basaltic centers, including  $\sim 3.7$  Ma centers (light gray shading), and north-northeast-aligned  $\sim 1.0$  Ma centers (black, along trend shown by dashed line) and Lathrop Wells cone (black). Location of the proposed repository is just east of Mile. Main shock focal mechanism of the Little Skull Mountain earthquake sequence (lower hemisphere, black indicates compressional first motion) is shown at the epicenter, with average orientation of P and T axes of the sequence (point and arrows marked P and T, respectively) from (9).

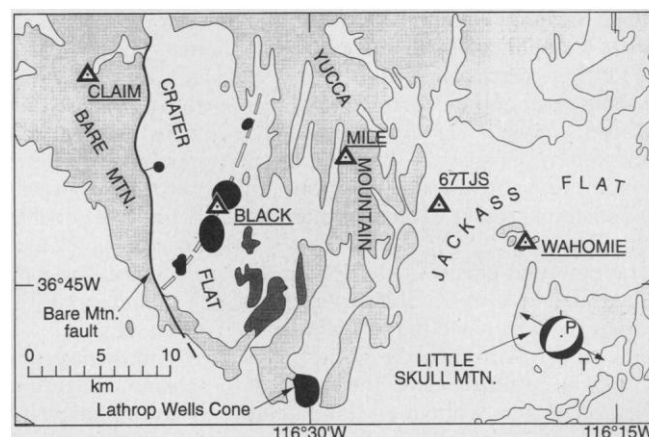
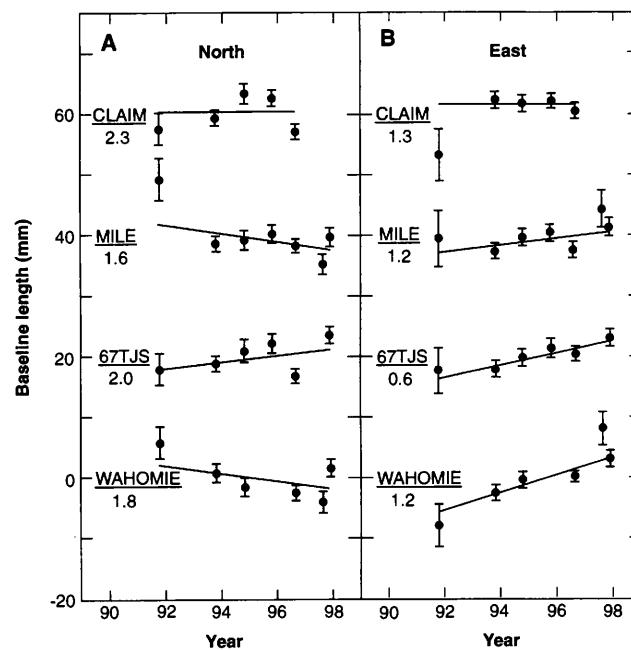


**Fig. 2.** Time series of site position estimates for the (A) north and (B) east components of the GPS data. To establish a geodetic reference frame for this figure, the time-dependence of the position of site Black is constrained to follow a linear trend exactly (the estimates for this site are therefore not shown), such that the regressed slope of Claim is zero. The intersite velocities and scaled uncertainties quoted in the text and in Fig. 3 are not dependent on the choice of reference frame. The error bars are the scaled standard deviations (12). Positions are shown relative to an arbitrary reference value. The lines represent the best fit linear models, with normalized root-mean-square values shown below each site name.



B. Wernicke, M. J. Abolins, R. J. Brady, M. A. House, N. A. Niemi, J. K. Snow, Division of Geological and Planetary Sciences, California Institute of Technology, Pasadena, CA 91125, USA.

J. L. Davis, R. A. Bennett, P. Elósegui, Harvard-Smithsonian Center for Astrophysics, Cambridge, MA 02138, USA.

of 10 measurements during 1983 to 1997 (Fig. 4) (15). A weighted least-squares analysis of the 14-year record of Wahomie-Mile baseline lengths yields a linear trend of  $0.93 \pm 0.18$  mm/year (lengthening), consistent with our 1991 to 1997 GPS results, and significant with effectively 100% confidence.

The principal issues in evaluating the geophysical significance of these velocities is whether they represent steady-state strain accumulation, or whether all or part of the motion reflects other processes including (i) coseismic or rapid postseismic deformation (for example, afterslip or viscous relaxation) associated with the Little Skull Mountain earthquake, (ii) monument instability or other sources of time-correlated error, (iii) error in correcting for the GPS-geodolite scale difference, or (iv) undetected GPS error. The last three effects are difficult to evaluate because we have no expectation of how they would contaminate the secular rates for these particular sites. It is unlikely that some or all of these factors would have coincided to yield significant rates, the strain pattern apparent in Fig. 3B, or the expected west-northwest elongation, but they remain important caveats in interpreting the data.

The potential effects of the earthquake are quantifiable. Using a dislocation model in which it was assumed that the southeast-dipping nodal plane was the failure plane (10, 11) we estimate that the coseismic elongation of the Wahomie-Mile baseline

was  $\sim 7$  mm (16). Alternatively, if the northwest-dipping nodal plane is the slip plane (10) we obtain a coseismic baseline length change of  $< 1$  mm. The effect of coseismic motion on the other four sites is  $< 1$  mm for either nodal plane.

To assess the sensitivity of our Mile-Wahomie horizontal velocity estimate to assumptions regarding coseismic length changes, we fit three additional models to the Mile-Wahomie data set. For the first, we estimated the baseline length rate conditioned on the dislocation model for the southeast-dipping plane. The resulting rate estimate is  $0.66 \pm 0.18$  mm/year. For the second, we estimated the baseline length rate conditioned on the northwest-dipping nodal plane. The resulting rate estimate is  $0.91 \pm 0.18$  mm/year. Finally, we estimated both the baseline length rate and the coseismic offset directly from the Mile-Wahomie data set, allowing the rate and offset to be free parameters, which yielded  $0.83 \pm 0.22$  mm/year and  $2.6 \pm 3.1$  mm, respectively. To account completely for the estimated Wahomie-Mile rate with coseismic motion, an offset of 23 mm is required, resulting in a  $\chi^2$ -per-degree-of-freedom of 6.8. For any reasonable treatment of the earthquake, the measured baseline lengths exclude the "no-motion" hypothesis (rate of 0.0 mm/year) with greater than 99% confidence (17).

Transient post-seismic strain, such as afterslip or flexure in response to viscous relaxation, are well known from large earthquakes. Displacements related to these effects tend to be either undetectable or a small fraction of the coseismic displacement, and significant only within a few rupture dimensions of the fault (18), and so are likely to be of consequence only at Wahomie and perhaps 67TJS. For example, a nominal afterslip of 10% on the southeast-dipping plane accommodated within the first year after the earthquake would result in an elongation of the Wahomie-Mile baseline of only 0.7 mm, which is a

small fraction of the scatter in the data about the best-fit line (Fig. 4). Hence, if the observed rates are indeed a transient post-seismic effect, they would be anomalously large, long-lasting, and areally extensive for a  $M_s$  5.4 earthquake, particularly as regards the velocities of sites west of Wahomie.

To test the consistency among the GPS-determined baseline lengths, the trilateration-determined baseline lengths, and our regression models, we estimated rates using the GPS-determined lengths only. A weighted least-squares analysis yields an estimate for the Wahomie-Mile length rate of  $0.88 \pm 0.23$  mm/year (no earthquake). The difference between the rates estimated with and without the trilateration observations [using the method of (19)] is not significant ( $0.05 \pm 0.14$  mm/year), confirming compatibility of the trilateration and GPS data sets under the assumption of no significant motion as a result of the earthquake. GPS rate estimates conditioned on southeast-dipping and northwest-dipping earthquake models are equivalent at  $0.80 \pm 0.23$  and  $0.87 \pm 0.23$  mm/year, respectively, illustrating that the Wahomie-Mile GPS observations alone are insensitive to the earthquake.

Bearing in mind the caveats that an anomalous process related to the earthquake or an improbable combination of error sources may have contributed to the observed rates (20), we interpret the results to reflect secular intersite motions of  $\sim 1$  mm/year. If the strain field is essentially uniform extension  $N70^\circ W$  and the secular rate between Wahomie and Claim is 1.7 mm/year, then the strain rate is 51 nstr/year, about three to four times the average Basin and Range rate and about one-fourth of the highest strain accumulation rates in the United States (21).

Rates of this magnitude are difficult to reconcile with the Quaternary history of earthquakes and volcanism in the Yucca Mountain area. Horizontal offsets are typically 1 to 2 m for significant ( $M_s > 7.0$ )

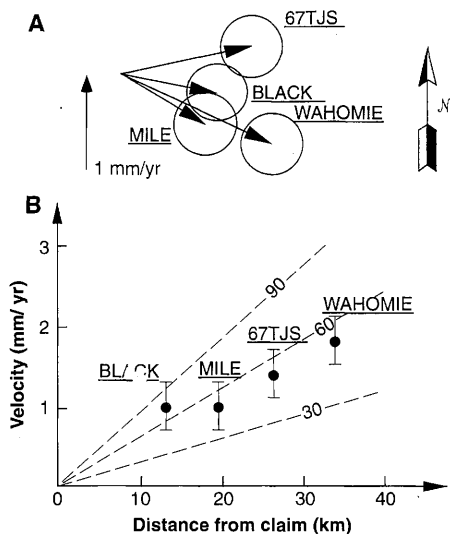
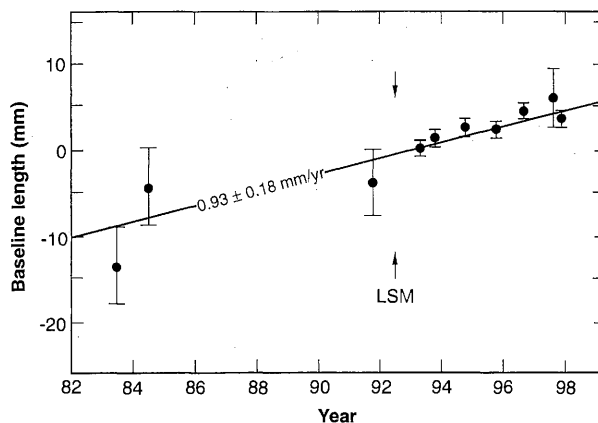


**Fig. 3.** (A) Plot showing horizontal velocities (vectors) and scaled  $1\sigma$  error ellipses (12) for sites Black, Mile, 67TJS, and Wahomie relative to Claim, based on 1991 to 1997 GPS surveys. (B) Plot showing horizontal velocities and scaled standard deviations from (A) versus distance from Claim, showing contour lines in nanostrains per year for a uniform strain model.

**Fig. 4.** Time series of Wahomie-Mile line lengths with scaled  $1\sigma$  errors (12), showing best fit straight line. Arrows labeled LSM show the time of the 29 June 1992 Little Skull Mountain earthquake.



Basin and Range earthquakes (22); thus if the rate were steady there should be 5 to 50 large earthquakes every 10,000 to 100,000 years. The only candidate for such a fault in the area is the Bare Mountain fault, which appears to have experienced only one significant earthquake in the last 10,000 years, and likely only two events since ~150 ka (6). Estimated slip rates for the Bare Mountain fault are 0.02 to 0.20 mm/year (8), one to two orders of magnitude lower than expected if the contemporary rates were sustained through the late Quaternary. Although some of the faults on Yucca Mountain have demonstrable late Quaternary slip, the total slip is only 0.002 to 0.020 mm/year (8).

The strain pattern is also difficult to reconcile with shear related to the north-west-trending Death Valley fault zone, some 35 km southwest of our array. It has a GPS-determined slip rate of 3 to 5 mm/year (14), and therefore shear strain rates related to the fault in excess of ~10 nstr/year would be unlikely in the Yucca Mountain area.

Speculatively, strain accumulation across the area could be driven by magmatic inflation at depth (23). A tomographic study of the area hints that a low-velocity zone may be present in the deep crust beneath Crater Flat, consistent with the presence of basaltic magma (24). Dikes associated with low-volume basaltic magmatism in the upper continental crust are typically 1 to 3 m wide (25); thus 5 to 50 dike events would be required every 10,000 to 100,000 years to account for the observed strain. Therefore, unless the youngest eruptive center, the Lathrop Wells cone, reflects an extensive system of upper crustal dikes that do not break the surface, the volcanic history of the area does not reflect an average strain rate of 50 nstr/year. Such a rate over the last million years would have resulted in the relatively steady intrusion of some 500 to 1000 dikes.

We suggest that the apparent inconsistency between the observed contemporary rates and the geologic history is because the Yucca Mountain area is experiencing an epoch of anomalously rapid strain accumulation. The integrated strain across the Basin and Range (length scale of ~1000 km) may be continuous at the million-year time scale, but local magmatic and tectonic events within the province (length scale of ~100 km) may be strongly clustered in both space and time, and have recurrence times or repose intervals of a few thousand to hundreds of thousands of years [for example (4, 26)]. If the contemporary strain rate in the Yucca Mountain area is any indication, elastic strain accumulation related to these events may also be strongly episodic. An event of duration 100,000 years occurring every million

years would accord well with the overall tectonic and volcanic history. If so, hazard analyses based on the local record of magmatic and tectonic events alone would underestimate the probability of such events occurring in the near future at Yucca Mountain by an order of magnitude. For example, the anomalous strain could reflect the development of a second line of north-northeast aligned, low-volume eruptive centers, analogous to the cluster of events near 1.0 Ma on Crater Flat, with the eruption of the Lathrop Wells cone representing the onset of a cluster that would continue over the next few tens of thousands of years (27).

## REFERENCES AND NOTES

- R. B. Scott, *Geol. Soc. Am. Mem.* **176**, 251 (1990).
- V. A. Frizzell and J. Shulters, *U.S. Geol. Surv. Map I-2046* (1990).
- C. B. Connor and B. E. Hill, *J. Geophys. Res.* **100**, 10107 (1995).
- R. J. Fleck *et al.*, *ibid.* **101**, 8205 (1996).
- S. G. Wells, L. D. McFadden, C. E. Renault, B. M. Crowe, *Geology* **18**, 549 (1990); M. G. Zreda, F. M. Phillips, P. W. Kubik, P. Sharma, D. Elmore, *ibid.* **21**, 57 (1993).
- M. C. Reheis, *U.S. Geol. Surv. Bull.* **1790**, 103 (1988).
- The steeply east-dipping Bare Mountain fault zone is >20 km long, has an estimated 2 km of vertical offset [D. B. Snyder and W. J. Carr, *J. Geophys. Res.* **89**, 10193 (1984); S. A. Monsen, M. D. Carr, M. C. Reheis, P. A. Orkild, *U.S. Geol. Surv. Map I-2201* (1992)] and demonstrable late Quaternary slip (6).
- Quaternary slip occurred on most of the major faults at Yucca Mountain, but only one (the Windy Wash fault) has yielded a Quaternary slip rate, which was ~0.002 mm/year, based on a 40-cm offset of a 0.27 Ma gravel [(1); J. W. Whitney, R. R. Shroba, F. W. Simonds, S. T. Harding, *Geol. Soc. Am. Abstr. Prog.* **16**, 787 (1984)]. Estimates of the total Quaternary fault slip rates in the Yucca Mountain area are 0.02 to 0.20 mm/year (R. McGuire, in C. B. Raleigh *et al.*, *Ground Water at Yucca Mountain; How High Can It Rise?* (National Research Council, Washington, DC, 1992), Appendix E; K. J. Coppersmith, R. R. Youngs, *Elec. Power Res. Inst. Rep. NP-7057* (1990); D. A. Ferrill *et al.*, *Geology* **24**, 559 (1996); L. W. Anderson, R. E. Klinger, D. S. Anderson, *ibid.* **25**, 189 (1997)].
- S. C. Harmsen, *Bull. Seismol. Soc. Am.* **84**, 1484 (1994).
- The epicenter of the Little Skull Mountain earthquake was directly beneath Little Skull Mountain [Fig. 1; (9); M. Meremonte, J. Gombert, E. Cranswick, *Bull. Seismol. Soc. Am.* **85**, 1039 (1995); K. D. Smith *et al.*, *ibid.*, in press. The focal mechanism indicated nearly pure normal slip; nodal planes dip northwest and southeast. The focus was at a depth of ~10 km, and aftershocks were clustered at depths of 7 to 10 km. The size of the event and the aftershock distribution suggest that the rupture zone was relatively small (~25 km<sup>2</sup>) and deep. Most of the aftershocks crudely align along the southeast dipping plane, suggesting that it was the rupture plane. Alternatively, the prevailing northwesterly dip of surface faults would suggest that the northwest-dipping plane was the rupture plane. In particular, the northwest-dipping Rock Valley fault zone, which lies southeast of the epicenter and is defined by a number of significant Quaternary fault scarps (2), is the only known Quaternary surface rupture updip from either focal plane.
- J. C. Savage, M. Lisowski, W. K. Gross, N. E. King, J. L. Svarc, *J. Geophys. Res.* **99**, 18103 (1994). The 50 nstr/year maximum is based on the 2 $\sigma$  upper bound of east-west elongation in their table 2, and is slightly higher than the maximum reported shear strain rate. The 1993 geodolite survey also included GPS observations using Ashtech series LM-XII receivers. Significant motion was detected for one site located in the epicentral area of the Little Skull Mountain earthquake, which did not affect any of the other sites at the level of precision of the measurements.
- All surveys were conducted using Trimble 4000 series GPS receivers with compact L1/L2 ground-plane antennas, positioned with an optical plummet on a tripod, and included slant-height and plumb-bob checks before and after each survey to verify vertical position above the mark. Antenna heights were generally 0.9 to 1.4 m above the mark. Field procedures followed protocols developed by the University Navstar Consortium (UNAVCO). Each campaign included between 8 and 24 hours of data collection with a 15- or 30-s measurement interval. GPS phase data were reduced using the GAMIT software [R. W. King and Y. Bock, "Documentation for the MIT GPS analysis software: GAMIT, Technical report" (Massachusetts Institute of Technology, Cambridge, MA, 1995)]. To account for errors in modeling the phase measurements, the 2 to 3 mm "formal" uncertainties generally assumed for phase data were scaled a priori up to 10 mm. Uncertainties for GAMIT site position estimates are therefore approximately four times greater than the formal uncertainties. The GLOBK analysis software [T. A. Herring, "GLOBK: Global Kalman filter VLBI and GPS analysis program, Technical report" (Massachusetts Institute of Technology, Cambridge, MA 1995)] was used to combine position estimates for the different epochs to estimate velocities in a global reference frame. At this stage, we used global tracking data, ranging from 11 sites in 1991 to 137 sites in 1997, from the International GPS Service for Geodynamics, making use of data products provided by Scripps Orbit and Permanent Array Center. After this stage, we evaluated the option of correcting the a priori phase uncertainty scale factor, which would be warranted on the basis of scatter of the data about the best-fit line. The standard measure of the scatter is the  $\chi^2$  statistic, where a  $\chi^2$  per degree of freedom greater than unity may indicate that the a priori scale factor underestimated unmodeled errors. For the Wahomie-Mile baseline series (Fig. 4), the  $\chi^2$  per degree of freedom is 0.75, indicating that the a priori scaling was conservative. Nevertheless, we chose not to reduce the uncertainties, but retained the more conservative a priori scaling.
- J. M. Stock and J. H. Healy, *U.S. Geol. Surv. Bull.* **1790**, 87 (1988).
- R. A. Bennett *et al.*, *Geophys. Res. Lett.* **24**, 3073 (1997). In addition to these five surveys (1991–1996), the solution presented here includes data from two additional surveys in 1997. The first 1997 survey included only Wahomie and Mile, and the second included all sites except Claim, which was destroyed by mining activity. The 1995 Wahomie-Mile baseline length estimate, which does not appear to be anomalous (Fig. 4), was nevertheless excluded from the rate estimate because of a possible error in the station setup at Wahomie.
- Before incorporation into the time series, trilateration measurements were modified for the GPS-trilateration scale difference, where geodolite distances are observed to be  $0.283 \pm 0.100$  parts per million of baseline length longer than GPS (J. C. Savage, M. Lisowski, W. H. Prescott, *J. Geophys. Res.* **191**, 547 (1996)). The correction is thus  $4.0 \pm 1.4$  mm of shortening of the Wahomie-Mile geodolite baseline lengths for 1983 and 1984.
- We calculated coseismic baseline length changes using the same method and hypocentral location as in (17), which assumed a 5-km<sup>2</sup> rupture plane centered at a mean depth of 8 km, with the focus along the bottom center of the plane and 58 cm of normal slip. We modeled the northwest-dipping plane with the same parameters but dipping 36°N55°W.
- We tested the lesser "no motion" null hypothesis, that is, that the time series can be explained by a two-parameter model that involves a constant mean baseline length and a coseismic offset at the epoch of the earthquake, against the fuller three-parameter model, which includes the baseline rate as a free

parameter, using the F-distributed model test statistic [equation 20 of R. A. Bennett, W. Rodi, R. E. Reilinger *J. Geophys. Res.* **101**, 21943 (1996)]. This test allows us to assess the level of complexity in the deformation model required to explain the baseline time series.

18. See C. H. Scholz, *The Mechanics of Earthquakes and Faulting* (Cambridge Univ. Press, Cambridge, 1990), chaps. 4 and 5, and references therein.
19. J. L. Davis, T. A. Herring, I. I. Shapiro, A. E. E. Rogers, G. Elgered, *Radio Sci.* **20**, 1593 (1985).
20. If the error sources serendipitously resulted in the observed  $\chi^2$  per degree of freedom of slightly less than unity (12), the "true"  $\chi^2$  per degree of freedom would be significantly less than unity.
21. The average rate across the entire Basin and Range is  $\sim 15$  to 20 nstr/year [for example, T. H. Dixon, S. Robaudo, J. Lee, M. C. Reheis, *Tectonics* **14**, 755 (1995); R. A. Bennett, B. P. Wernicke, J. L. Davis, *Geophys. Res. Lett.* **25**, 563 (1998)]. Rates of  $\sim 200$  nstr/year are typical along the San Andreas fault [for example, W. Thatcher, *U.S. Geol. Surv. Prof. Pap.* 1515 (1990)], p. 189.
22. R. E. Wallace, *J. Geophys. Res.* **89**, 5763 (1984); R. S. Stein, S. E. Barrientos, *ibid.* **90**, 11355 (1985); M. N. Machette, S. F. Personius, A. R. Nelson, *Ann. Tectonic.* **6** (suppl.), 5 (1992).
23. T. Parsons and G. A. Thompson, *Science* **253**, 1399 (1991).
24. J. R. Evans and M. Smith III, in *Major Results of Geophysical Investigations at Yucca Mountain and Vicinity, Southern Nevada*, H. W. Oliver, D. A. Ponce, W. Clay Hunter, Eds. [Open-File Report, U.S. Geological Survey, OF-0074 (1995)], pp. 135–156.
25. P. T. Delaney and A. E. Gartner, *Geol. Soc. Am. Bull.* **109**, 1177 (1997).

26. R. E. Wallace, *Bull. Seismol. Soc. Am.* **77**, 868 (1987).
27. E. I. Smith, D. L. Feuerbach, T. R. Nauman, J. E. Faults, *Proceedings of the International Topical Meeting, High-Level Radioactive Waste Management* (American Nuclear Society/American Society of Civil Engineers, Las Vegas, 1990), vol. 1, pp. 81–90.
28. We thank J. Savage and M. Lisowski for providing trilateration data and GPS data and results from their 1993 survey, and J. Savage for useful discussions. The University NAVSTAR Consortium provided equipment and field logistical support. This project was funded by Nuclear Regulatory Commission contracts NRC-04-92-071 and NRC-02-93-005, and National Science Foundation grant EAR-94-18784.

29 October 1997; accepted 3 March 1998

## Test of General Relativity and Measurement of the Lense-Thirring Effect with Two Earth Satellites

Ignazio Ciufolini, Erricos Pavlis, Federico Chieppa, Eduardo Fernandes-Vieira, Juan Pérez-Mercader

The Lense-Thirring effect, a tiny perturbation of the orbit of a particle caused by the spin of the attracting body, was accurately measured with the use of the data of two laser-ranged satellites, LAGEOS and LAGEOS II, and the Earth gravitational model EGM-96. The parameter  $\mu$ , which measures the strength of the Lense-Thirring effect, was found to be  $1.1 \pm 0.2$ ; general relativity predicts  $\mu \equiv 1$ . This result represents an accurate test and measurement of one of the fundamental predictions of general relativity, that the spin of a body changes the geometry of the universe by generating space-time curvature.

Einstein's general theory of relativity (1, 2) predicts the occurrence of peculiar phenomena in the vicinity of a spinning body, caused by its rotation, that have not yet been measured (3). When a clock that co-rotates very slowly around a spinning body returns to its starting point, it finds itself advanced relative to a clock kept there at "rest" (with respect to "distant stars"). Indeed, synchronization of clocks all around a closed path near a spinning body is not possible, and light co-rotating around a spinning body would take less time to return to a fixed point than light rotating in the opposite direction (2). Similarly, the orbital period of a particle co-rotating around a spinning body would be longer than the orbital period of a particle counter-rotating on the same orbit. Furthermore, an orbiting particle around a spinning

body will have its orbital plane "dragged" around the spinning body in the same sense as the rotation of the body, and small gyroscopes that determine the axes of a local, freely falling, inertial frame, where "locally" the gravitational field is "unobservable," will rotate with respect to "distant stars" because of the rotation of the body. This phenomenon—called "dragging of inertial frames" or, more simply, "frame dragging," as Einstein named it—is also known as the Lense-Thirring effect (1, 2, 4). In Einstein's general theory of relativity, all of these phenomena are the result of the rotation of the central mass.

Rotation, inertia, and the "fictitious" inertial forces arising in a rotating system have been central issues and problems of mechanics since the time of Galileo and Newton (5). Mach thought that the centrifugal forces were the result of rotation with respect to the masses in the universe, and Einstein's development of the general theory of relativity was influenced by Mach's ideas on the origin of inertia and inertial forces. Today, the level at which general relativity satisfies Mach's ideas on inertia is still debated and discussed. However general relativity satisfies at least a kind of "weak manifestation" of Mach's

ideas: the dragging of inertial frames (2). Indeed, in Einstein's gravitational theory, the concept of an inertial frame has only a local meaning, and a local inertial frame is "rotationally dragged" by mass-energy currents because moving masses influence and change the orientation of the axes of a local inertial frame (that is, the gyroscopes); thus, a current of mass such as the spinning Earth "drags" and changes the orientation of the gyroscopes with respect to the distant stars.

To understand these phenomena of general relativity associated with the rotation of a mass, one may use a formal analogy with the classical theory of electromagnetism. Newton's law of gravitation has a formal counterpart in Coulomb's law of electrostatics; however, Newton's theory has no phenomenon formally analogous to magnetism. On the other hand, Einstein's theory of gravitation predicts that the force generated by a current of electrical charge, described by Ampere's law, should also have a formal counterpart "force" generated by a current of mass. The detection and measurement of this "gravitomagnetic" force is the subject of this report.

The gravitomagnetic force causes a gyroscope to precess with respect to an asymptotic inertial frame with angular velocity  $\dot{\Omega} = -\frac{1}{2}\mathbf{H} = [-\mathbf{J} + 3(\mathbf{J}\cdot\hat{\mathbf{x}})\hat{\mathbf{x}}]/|\mathbf{x}|^3$ , where  $\mathbf{H}$  is the gravitomagnetic field,  $\mathbf{J}$  is the angular momentum of the central object, and  $\mathbf{x}$  is the gyroscope's position vector. This formula quantifies the Lense-Thirring effect for a gyroscope (1, 2). The gravitomagnetic force also causes small changes in the orbit of a test particle (4). In particular, there is a secular rate of change of the longitude of the nodes (intersection between the orbital plane of the test particle and the equatorial plane of the central object) given by  $\dot{\Omega}^{\text{Lense-Thirring}} = 2J/[a^3(1-e^2)^{3/2}]$ , where  $a$  is the semimajor axis of the test particle's orbit and  $e$  is its orbital eccentricity. In addition, there is a secular rate of change of the longitude of the pericenter (2),  $\dot{\omega}$  (determined by the Runge-Lenz vector):  $\dot{\omega}^{\text{Lense-Thirring}} = 2J[\hat{\mathbf{J}} -$

I. Ciufolini, Istituto Fisica Spazio Interplanetario-Consiglio Nazionale delle Ricerche, and Dipartimento Aerospaziale, Università di Roma "La Sapienza," via Eudossiana 16, 00184 Rome, Italy.

E. Pavlis, Joint Center for Earth System Technology, University of Maryland-Baltimore County, Baltimore, MD 21250, USA.

F. Chieppa, Scuola Ingegneria Aerospaziale, Università di Roma "La Sapienza," Rome, Italy.

E. Fernandes-Vieira and J. Pérez-Mercader, Laboratorio de Astrofísica Espacial y Física Fundamental (INTA-CSCIC), Madrid, Spain.